Polymer, Volume 50, Issue 23, 3 November 2009, Pages 5539-5548

Accepted Manuscript

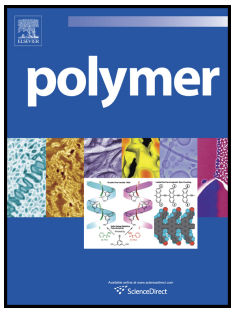

Title: Notched impact behavior of polymer blends: Part 1: New model for particle size dependence

Authors: C.B. Bucknall, D.R. Paul

PII: S0032-3861(09)00816-7

DOI: 10.1016/j.polymer.2009.09.059

Reference: JPOL 13491

To appear in: *Polymer*

Received Date: 7 July 2009

Revised Date: 15 September 2009

Accepted Date: 18 September 2009

Please cite this article as: Bucknall CB, Paul DR. Notched impact behavior of polymer blends: Part 1: New model for particle size dependence, Polymer (2009), doi: 10.1016/j.polymer.2009.09.059

1st Sep 2009

Notched impact behavior of polymer blends: Part 1: New model for particle size dependence

C.B. Bucknall[a,*], D.R. Paul[b,*]

[a]SAS B61, Cranfield University, Bedford MK43 0AL, UK

[b]Department of Chemical Engineering and Texas Materials Institute, The University of Texas at Austin, Austin, TX 78712, USA

A model is proposed to explain the observed relationships between particle size and fracture resistance in high-performance blends, which typically reach maximum toughness at particle diameters of 0.2-0.4 μm. To date there has been no satisfactory explanation for the ductile-brittle (DB) transition at large particle sizes. The model is based on a recently-developed criterion for craze initiation, which treats large cavitated rubber particles as craze-initiating Griffith flaws. Using this criterion in conjunction with Westergaard's equations, it is possible to map the spread from the notch tip of three deformation mechanisms: rubber particle cavitation, multiple crazing and shear yielding. Comparison of zone sizes leads to the conclusion that maximum toughness is achieved when the particles are large enough to cavitate a long way ahead of a notch or crack tip, but not so large that they initiate unstable crazes and thus reduce fracture resistance.

Keywords: Impact modified polymers; Toughening; Structure/property relationship

*To whom correspondence should be addressed: E-mail: clivebucknall@aol.com; drp@che.utexas.edu

1. Introduction

It has long been known that the impact resistance of rubber toughened polymers is strongly dependent upon the concentration, size and size distribution of the rubber particles [1]. This knowledge has underpinned the development of a wide range of commercially successful products over the past 50 years. A good general rule is that small particles (weight-average diameters D_w in the range 0.2–0.4 μm) work well when shear yielding dominates the toughening mechanism, whereas larger particles (D_w between 2 and 3 μm) are more effective when multiple crazing is the principal mechanism of energy absorption.

For any given blend composition, maximum toughness is restricted to a limited range of particle sizes, which is often quite narrow. Moving beyond the preferred range in either direction results in a ductile-brittle transition, as illustrated in Figure 1, where **b** and **d** respectively mark the midpoints of the lower and upper transitions and thus define critical particle sizes. The curve is based on results for a specific rubber-toughened nylon 6 (RTPA6) blend [2], but with appropriate scaling of particle size and peak height, similar curves could be drawn for almost any well-made rubber-toughened polymer.

For many years, interest in particle size effects came mainly from polymer manufacturers, who were best placed to carry out the necessary experiments. However, the introduction of 'supertough' nylons by DuPont [3-4] in the late 1970s attracted the attention of the wider scientific community, for two reasons. First, the new blends were made by the novel process of reactive compounding, which is a relatively simple method for preparing blends with controlled particle sizes. Second, the relationships between impact behavior and particle size in RTPA6.6 blends proved to be far from simple [5-6].

As a result of the interest generated by the first publications in this area, there is now a substantial body of literature describing the effects of particle size on impact behavior in a wide range of polyamides [5-25], and in a more limited range of thermoplastic polyesters [26-30]. Polypropylene blends present a greater challenge because of their low chemical reactivity and more restricted range of average particle sizes, but have nevertheless been the subjects of several investigations [31-35].

This research was stimulated by the pioneering work of Wu, who prepared PA6.6 blends containing 10%, 15% and 25% of grafted polyolefin rubber. He varied average particle sizes from 0.3 to 3.0 μm, and (as expected) observed DB transitions similar to the one shown in section **c-e** of Figure 1. However, against expectation he also found that the critical average particle size $<D>_{crit}$ increased systematically with rubber content. On this basis Wu concluded that average particle size was not the primary factor governing impact resistance. Instead, he advocated using average inter-particle spacing $<d_{ip}>$ as a more fundamental parameter, where d_{ip} is the smallest distance between the surfaces of neighboring particles.

To calculate $<d_{ip}>$ Wu made two simplifying assumptions: that all particles have the same diameter D, and that the particles form a regular cubic array. The resulting expression is:

$$< d_{ip} > = D\left[\left(\frac{\pi}{6\phi_p}\right)^{1/3} - 1\right] \qquad (1)$$

where ϕ_p is the volume fraction of rubber particles. His plots of Izod impact energy against $log<d_{ip}>$ showed that the upper DB transition occurred at the same estimated critical inter-particle spacing in all three sets of RTPA6.6 blends. Subsequently, Wu made provision for the distribution of particle sizes in melt-compounded blends, and introduced the term 'matrix ligament thickness' to describe $<d_{ip}>$, in order to shift the focus from the rubber particles to the matrix material [36]. Margolina and Wu postulated that shear yielding occurs only in ligaments below a critical thickness, and that general yielding takes place when $<d_{ip}>$ is below a critical mean matrix ligament thickness $<d_{ip}>_{crit}$, so that plastic deformation percolates across the specimen. These ideas have been extended and elaborated over the years [37-42].

One consequence of increasing rubber content (thereby reducing $<d_{ip}>$) is an increase in local stress concentrations, as the stress fields surrounding individual particles begin to overlap. This has led to suggestions that the inter-particle spacing effect has its origins in stress field overlap [7, 43]. In evaluating these suggestions, it is important to differentiate between reductions in $<d_{ip}>$ due to increases in ϕ_p and those due to reductions in D. A higher volume fraction of soft particles inevitably raises stress concentrations in the matrix, because the same loads are borne by a smaller cross-sectional area. By contrast, changing particle

size has no effect on local stress concentrations, provided that the volume fraction and degree of dispersion are held constant. Put simply, there are no length scales in finite element analysis; if all linear dimensions, including particle size and interparticle spacing, are changed by the same ratio, the pattern of stresses across the region under analysis remains unchanged. Clearly the impact behavior reported by Wu cannot be explained by stress field overlap.

Following Wu's work, Gaymans, Borggreve and co-workers extended the study to include blends with very small particles, and impact tests at various temperatures [8-13, 26]. They showed that RTPA6 exhibits both a lower and an upper DB transition, and that the upper critical particle size defined by point **d** in Figure 1 is temperature-dependent, varying continuously from 0.5 μm at −10°C to 1.5 μm at 50°C in RTPA6 blends containing 20 wt % of grafted EPDM rubber. Extensive subsequent work has demonstrated the existence of a minimum rubber particle size for toughening in other semi-crystalline polyamides [17], amorphous nylon (a-PA) [2, 44], poly(methyl methacrylate) (PMMA) [45], poly(vinyl chloride) (PVC) [46-47] and PA6 containing a variety of different elastomers [22-25].

Previous attempts to interpret the impact behavior of these 'supertough' blends have met with mixed success. There is general agreement that very small particles are ineffective because they are more resistant to cavitation, but to date there has been no convincing explanation for the upper DB transition. Muratoglu, Argon and Cohen have argued that super-tough behavior in RTPA6 blends is due to an oriented crystalline layer of limited thickness (~ 0.15 μm) which extends radially from the surface of each rubber particle [48-51]. However, this hypothesis is not consistent with the strong relationship observed by Gaymans and co-workers between critical particle size and temperature, nor with recent work by Huang et al, which shows that the impact behavior of 80/20 rubber-toughened blends based on the amorphous nylon Zytel 330 is very similar to that of 80/20 blends based on PA6 [2, 44, 52].

Despite this growing body of evidence, the inter-particle spacing theory still has its supporters. Recent articles by Corté and Leibler claim that high levels of toughening are extremely difficult to achieve in glassy polymers, and that lamellar crystalline structure in semi-crystalline polymers accounts for the dependence of impact resistance on inter-particle spacing [53-54]. Neither of these claims is valid. Supertough blends based on glassy

polymers have been available commercially since 1958, when core-shell particles were first used to make rubber-toughened PVC blends [55-56] . Another very successful family of non-crystalline supertough polymers comprises rubber-toughened blends based on polycarbonate [57-60], which were first introduced in the 1960s. There are numerous other examples of high-performance blends based on glassy polymers. The work of Huang et al on amorphous nylon comprehensively undermines the second claim. Furthermore, the results published by Corté and Liebler show that critical inter-particle spacings in PA6.6 and PA12 increase linearly with particle diameter and vary inversely with the square of the shear yield stress [54]. These findings demonstrate that there is no advantage in using d_{ip} rather than D as a basis for comparing impact data, especially as D is much easier to measure experimentally.

In light of this evidence, there are sound reasons for abandoning the concept of inter-particle spacing altogether. The alternative is to base all discussions of impact behavior on the size and volume fraction of rubber particles, which are known to affect fracture resistance in all polymer blends. From this perspective, any correlations involving spacings should be regarded as purely fortuitous.

The aim of the present article is to introduce a new model for deformation and fracture in polymer blends, which explains the observed impact behavior without relying on unnecessary hypotheses involving d_{ip}.

2. Yielding near notch tips

To understand the fracture resistance of polymer blends, it is first necessary to analyze their deformation behavior close to the tip of a sharp notch. The standard method is to apply Westergaard's crack tip stress field equations [61], as follows:

$$\sigma_1 = \frac{K_1}{\sqrt{2\pi r}}\cos\frac{\theta}{2}\left(1+\sin\frac{\theta}{2}\sin\frac{3\theta}{2}\right)+.... \quad (2a)$$

$$\sigma_2 = \frac{K_1}{\sqrt{2\pi r}}\cos\frac{\theta}{2}\left(1-\sin\frac{\theta}{2}\sin\frac{3\theta}{2}\right)+.... \quad (2b)$$

$$\sigma_{12} = \frac{K_1}{\sqrt{2\pi r}}\sin\frac{\theta}{2}\cos\frac{\theta}{2}\cos\frac{3\theta}{2}.... \quad (2c)$$

$$\sigma_3 = \nu\left(\sigma_1+\sigma_2\right) \qquad in\ \ plane\ \ strain \quad (2d)$$

$$\sigma_3 = 0 \qquad in\ \ plane\ \ stress \quad (2e)$$

where r and θ are polar coordinates with their origin at the crack tip, and θ = 0 on the crack plane. Axis 1 is the direction of applied stress, axis 2 is along the crack plane, and axis 3 is parallel to the crack tip; the shear stresses σ_{12} act on planes at θ = 45°. Most fracture mechanics textbooks combine von Mises' yield criterion with these equations to map the boundaries of the resulting shear yield zone [62-65]. Using this principle, r_p, the radius of the plastic zone on the crack plane (θ = 0) is then given by:

$$r_p = \frac{1}{2\pi}\left(\frac{K_I}{\sigma_{1y}}\right)^2 \qquad (3)$$

where K_I = stress intensity factor and σ_{1y} = first principal stress at yield. Provided the material near the crack tip is an elastic-plastic continuum, if follows that:

$$r_p = \frac{1}{2\pi}\left(\frac{K_I}{\sigma_y}\right)^2 \qquad \textit{in plane stress} \qquad (4)$$

$$r_p = \frac{1}{2\pi}\left(\frac{(1-2\nu)K_I}{\sigma_y}\right)^2 \qquad \textit{in plane strain} \qquad (5)$$

where σ_y = tensile yield stress and ν = Poisson's ratio. Since ν = 0.4 in a typical rigid polymer, the calculated plastic zone radius in plane stress is higher by a factor of 25 than r_p in plane strain. It has long been recognized that the simplified treatment outlined above leads to an underestimate of r_p, because it makes no provision for the redistribution of stress that inevitably follows crack tip plasticity. A simple method of overcoming this problem is to apply Irwin's correction, which specifies that the r_p values given by equations 3-5 should be doubled [66].

Since blends containing high concentrations of cavitated rubber particles cannot be described as continua, equations 4 and 5 do not apply to them. Free from the constraints of continuum mechanics, the cavitated plastic zones formed in polymer blends are able to increase substantially in radius even under plane strain conditions. They are by no means unique in this respect; microvoid nucleation and growth confer the same advantages on ductile metals [67]. Any analysis of plastic zone size must be based on yield criteria for porous solids.

Whatever corrections and adjustments are made in calculations of the type outlined above, the values of r_p obtained are at best only approximate; where accurate values are required, it is necessary to use laborious numerical methods. However, as the main emphasis in the present study is on understanding general trends rather than making precise predictions, there are many advantages in adopting a simplified approach. With this in mind, the present study first combines equations 2a-2d with a critical stress criterion for void formation to produce a series of maps of cavitation around a crack tip, for blends with a range of rubber particle sizes under plane strain loading. The same procedure is then applied to dilatational shear yielding in the resulting cavitated zone, and to multiple crazing initiated by the larger cavitated particles. By comparing maps produced in this way, it is possible to determine the sequence of events in each blend, and hence gain an insight into the effects of particle size on fracture behavior.

2.1 Rubber Particle Cavitation

The criteria for cavitation in rubber-toughened polymers have been modeled by Lazzeri and Bucknall [68-70], using energy-release rate principles similar to those used in fracture mechanics. Void formation and expansion in rubber particles are accompanied by the formation of new surface, stretching of the surrounding layers of rubber, and stress relaxation in the adjacent matrix. To calculate energy changes, the Lazzeri-Bucknall model treats blends as assemblies of small volume elements, each consisting of a spherical rubber particle of radius R surrounded by a concentric rigid elastic shell of outer radius Q, so that $\phi_p = R^3/Q^3$. The total energy released can then be calculated from the potential energy of the element before and after cavitation. The governing equation is:

$$U_p(r_{vd},\varepsilon_v) = \frac{2}{3}\pi R^3 K_r \left(\varepsilon_v - \frac{r_{vd}^3}{R^3}\right)^2 + 4\pi r_{vd}^2 \Gamma_r + 2\pi r_{vd}^3 G_r f\left(\lambda_f\right) \qquad (6)$$

where $U_p(r_{vd},\varepsilon_v)$ = potential energy of the rubber particle; r_{vd} = radius of void; ε_v = current volume strain of the particle (including the void); R = particle radius; G_r , K_r = shear and bulk moduli of rubber; Γ_r = surface energy of rubber; λ_f = extension ratio of the rubber at fracture in biaxial tension.

Calculations based on this model show that $\varepsilon_v(cav)$, the critical volume strain at cavitation, increases as the particle size is reduced, essentially because the strain energy

release rate is dependent on the size of the local volume element. When G_r is small, the relationship between *log* $\varepsilon_v(cav)$ and *log* D_p is approximately linear, as shown in Figure 2 [71-72]. The dotted line was obtained using equation 6, with G_r = 0.1 MPa, K_r = 2 GPa, Γ_r = 35 mJ m^{-2}, and ε_v held constant during cavitation to simplify the calculations; the energy released by the matrix was not taken into account.

Figure 2 compares a line calculated in this way with data obtained by Dompas et al, who confirmed that $\varepsilon_v(cav)$ is a function of particle size. Using a series of transparent PVC blends [46], these authors showed that a decrease in D_p caused an increase in critical strain to a maximum at $\varepsilon_v(cav)$ = 0.0128, where the specimens yielded before cavitation at a tensile stress of ~55 MPa and an elongation of 0.08. There are strong indications that similar relationships between D and $\varepsilon_v(cav)$ apply to rubber-toughened polyamides and other blends containing soft rubber particles ($G_r \approx 0.1$ MPa), as predicted by equation 6. Apart from size, the most important factors affecting cavitation (and therefore toughness) are Γ_r, the specific energy required to form new surface, and G_r, the stiffness of the rubber in shear, which determines the work done in stretching the rubber shell.

To fit the experimental data of Dompas et al in Figure 2, it has been necessary to shift the original calculated curve upwards, to a level at which the critical volume strains at a given particle size are approximately double those indicated by the dotted line. Furthermore, an even larger upward shift would have been required if energy released by the matrix had been taken into account when calculating $\varepsilon_v(cav)$. A possible explanation for this large discrepancy is that the shear moduli of the experimental rubber particles were substantially larger than 1 MPa. However, there is no reason to expect particularly high moduli in these experimental rubbers. The main reason for underestimating $\varepsilon_v(cav)$ is almost certainly more fundamental: the original calculations did not allow for the effects of an energy barrier in restricting void formation. They were based on the assumption that stressed void-free particles are unstable whenever there is enough energy to form a void. The alternative possibility is that they are metastable, and that an energy barrier controls the transition from the fully-dense to the cavitated state [73].

Figure 3 illustrates the effects of particle size on cavitation around a crack tip, calculated using equation 6 with K_I = 1.0 MPa $m^{0.5}$ and values of $\varepsilon_v(cav)$ taken from the solid line in

Figure 2. With increasing *D*, the cavitated zone extends boldly outwards from the crack tip, which helps to explain the lower brittle-ductile transition illustrated in Figure 1. These results show that the transition can be explained without assuming that small particles are unable to cavitate. A more balanced view is that problems arise simply because $\varepsilon_v(cav)$ is high, which limits the size of the cavitated yield zone, thereby increasing the probability of brittle fracture. In the limit, $\varepsilon_v(cav)$ becomes so high that the void-free blend yields under plane strain conditions before reaching the particle cavitation stress. Instead, a craze will extend from the notch tip, and crack growth will initiate before a significant amount of energy has been absorbed in ductile deformation. For a typical blend with a Young's modulus E = 2 GPa and ν = 0.4, a K_{IC} of 1.0 MPa $m^{0.5}$ corresponds to a fracture surface energy G_{IC} = 420 J m^{-2}, which is sufficient to form and rupture a single mature craze.

2.2 Shear Yielding

The standard criterion for shear yielding in void-free rigid polymers is a pressure-modified version of von Mises' criterion [74]:

$$\sigma_e \geq \sigma_{y0} + \mu P \equiv \sigma_{y0} - \mu \sigma_m \qquad (7)$$

where σ_{y0} is the yield stress in pure shear (σ_m = 0), μ is the pressure coefficient, P is pressure, the effective stress σ_e is given by:

$$\sigma_e \equiv \sqrt{\frac{(\sigma_1 - \sigma_2)^2 + (\sigma_2 - \sigma_3)^2 + (\sigma_3 - \sigma_1)^2}{2}} \qquad (8)$$

and the mean stress σ_m is defined as follows:

$$\sigma_m = -P = \frac{\sigma_1 + \sigma_2 + \sigma_3}{3} = K_b \varepsilon_v \qquad (9)$$

where K_b is bulk modulus. Typical values of K_b at 23°C are 3.5 GPa for a glassy polymer and 2.0 GPa for a rubber.

In Figure 4 this criterion is applied to shear yielding on the crack plane near a crack tip in a void-free blend containing 20% by weight of soft rubber particles, with ν = 0.4 and μ = 0.36. Owing to density differences ϕ_p = 0.26. The matrix polymer is based on dry PA6, and

has a tensile yield stress σ_{yt} = 70 MPa, which corresponds to σ_{y0} = 78.4 MPa. Blending with 20% rubber reduces σ_{yt} to 51.5 MPa and σ_{y0} to 57.6 MPa. Under plane strain the construction line meets the pressure-modified von Mises curve at a mean stress of 100.4 MPa, where σ_e = 21.5 MPa, $\sigma_1 = \sigma_2$ = 107.6 MPa, and σ_3 = 86.0 MPa. Thus pressure sensitivity helps to alleviate the adverse effects of notch tip constraint on shear yielding.

The presence of voids makes polymers more pressure-sensitive. Gurson has modeled yielding in porous solids containing distributed small voids, and obtained the following modification of von Mises' criterion [75-76].

$$\sigma_e \geq \sigma_{yt}\left(1 - 2\phi_{vd}\cosh\left(\frac{3\sigma_m}{2\sigma_y}\right) + \phi_{vd}^2\right)^{0.5} \qquad (10)$$

where σ_{yt} = tensile yield stress of the rigid matrix and ϕ_{vd} = volume fraction of voids. Because the matrix is itself pressure sensitive, a further modification is necessary when applying this criterion to porous polymers. The simplest way to do this is to replace σ_{yt} with $(\sigma_{y0} - \mu\sigma_m)$ to give:

$$\sigma_e \geq \left(\sigma_{y0} - \mu\sigma_m\right)\left(1 - 2\phi_{vd}\cosh\left(\frac{1.5\sigma_m}{\sigma_{y0} - \mu\sigma_m}\right) + \phi_{vd}^2\right)^{0.5} \qquad (11)$$

In view of the problems inherent in modeling the mechanical properties of solids containing dispersed spherical voids or inclusions [77], it is necessary to treat equations 10 and 11 with due caution. They are useful in describing general trends, but cannot be relied on to give accurate predictions of yield stress as a function of void content. One way to compare these equations with predictions based on other models, or with experimental data, is to set σ_m = 0, which gives the following expression for yielding in pure shear:

$$\sigma_e = \sigma_{y0}(\phi_{vd}) = \sigma_{y0}(0)\left(1 - 2\phi_{vd} + \phi_{vd}^2\right)^{0.5} = \sigma_{y0}(0)(1 - \phi_{vd}) \qquad \textit{in pure shear} \qquad (12)$$

where $\sigma_{y0}(0)$ is the yield stress in pure shear for the void-free matrix, and $\sigma_{y0}(\phi_{vd})$ is the effective stress at yield of a porous solid with volume fraction ϕ_{vd} of voids. Under pure shear loading, a similar relationship can be used for void-free rubber-modified blends, with ϕ_p

replacing ϕ_{vd}. This substitution is justified because, in comparison to the rigid matrix, rubber particles offer negligible resistance to shear stresses, and therefore behave almost exactly like voids in pure shear. As shown in Figure 4, the differences between voids and well-bonded soft particles become apparent only when the composite is subjected to large dilatational stresses. It is therefore possible to generalize equation 12 so that it applies to polymer composites containing a total volume fraction ϕ of any type of soft inclusions, including soft solid rubber particles, or voids, or any combination of the two. The resulting expression is:

$$\sigma_{y0}(\phi) = \sigma_{y0}(0)(1-\phi) \qquad \textit{in pure shear} \qquad (13)$$

Equations 12 and 13 are simple rule-of-mixtures expressions which provide only first-order approximations to the yield behavior of isotropic porous solids and particulate composites. However, they are consistent with equations 10 and 11, and the four equations together provide a convenient basis for evaluating the effects of cavitation on yield behavior.

Figure 4 clarifies some of the key issues concerning the contribution of void formation to toughness in polymer blends. Cavitation is important in notched specimens because it enables the blend to yield at moderate stresses under plane strain conditions, not because it eliminates geometrical constraints and produces a state of plane stress, as some commentators have suggested. For the fully-cavitated blend, the plane strain line crosses the Gurson curve at σ_m = 52.1 MPa, σ_e = 11.1 MPa, which corresponds to a stress state (55.8, 55.8, 44.7), well below the yield stress for the same blend with solid rubber particles. These two sets of data are used later to illustrate the potential effects of large-scale cavitation on the radius of the shear yield zone.

The principles set out above are applied in Figure 5 to PA6 blends under tensile loading, where the lower solid curve was obtained using equation 11, on the assumption that all particles have cavitated but none has expanded after cavitation. In practice, some particles will always remain void free during the early stages of a tensile or notched impact test, while others in the same neighborhood cavitate and increase in volume. Figure 5 also shows experimental yield stress data on a RTPA6 blend containing 26% by volume of rubber particles [2], and predictions for dry PA6 blends containing solid rubber particles, which are based on the assumption that the relationship between σ_{yt} and ϕ_p is a rule of mixtures similar to that shown in equation 13:

$$\sigma_{yt}(\phi_p) = (1 - \phi_p)\,\sigma_{yt}(0) \qquad (14)$$

The dashed curve in Figure 5 indicates the effects of increasing void content on θ_b, the angle between the tensile axis and a line drawn normal to the plane of the shear band. The relationship between pressure sensitivity and θ_b, which is determined by the gradient of the plastic potential function, is discussed in detail by Ward [74]. Because cavitation increases pressure dependence, θ_b falls to zero when the void fraction reaches 0.53 [68]. This rotation of the band plane reduces resistance to crack tip opening; at $\theta_b = 0$, yielding occurs entirely in response to tensile stresses applied normal to the bands, which in that respect resemble crazes. Good examples of craze-like cavitated shear bands have been reported by Sue [78].

The problems arising in the absence of cavitation are illustrated in Figure 6, which compares envelopes for pressure-dependent shear yielding under plane stress and plane strain loading, at K_I = 1.0 MPa $m^{0.5}$ in a void-free polymer blend with a tensile yield stress of 51.5 MPa. As noted earlier, with E = 2 GPa and ν = 0.4, this corresponds to a strain energy release rate G_I of 420 J m^{-2}, which is sufficient to initiate crazing and crack growth in the plane strain region. Since the calculations used to generate these yield envelopes do not allow for stress redistribution, real plastic zone sizes in a material of this type are about double those shown. However, even when this adjustment is made, it is clear that the plane stress yield zone is not large enough to enable a standard notched Izod specimen to overcome its vulnerability to brittle fracture.

Cavitation enables the whole plastic zone, including the plane strain region, to respond to dilatational stresses by both expanding in volume and increasing in radius. To achieve maximum toughness, two conditions must be satisfied: extensive cavitation ahead of the crack tip, and maximum involvement of the matrix in plastic deformation, which includes yielding, cold-drawing and strain hardening. Another important requirement, except in the most robust matrix polymers (e.g. polyethylene), is full participation of the rubber phase in the strain hardening mechanism; to achieve this, the rubber particle must be strongly bonded to the matrix and to any internal occlusions. As discussed in Section 2.1, the extent of cavitation and hence the level of toughness achieved depend on particle size, degree of crosslinking in the rubber phase, surface energy, and test conditions (especially temperature and strain rate). To ensure that the matrix plays a full part in energy absorption, shear

yielding should be the predominant deformation mechanism, and the chains must be long enough to avoid premature failure. Blends that depend entirely on multiple crazing for their toughness do not exhibit supertough behavior.

2.3 Crazing

Recent work has shown that craze initiation is a frustrated fracture process which falls within the scope of linear elastic fracture mechanics [79]; therefore the appropriate criterion is the Griffith equation, with slightly modified nomenclature:

$$\sigma_{craze} = \sqrt{\frac{E\,G_{craze}}{Y^2\,\pi\,(1-\nu^2)\,a}} \qquad (15)$$

where σ_{craze} is the critical stress for craze initiation, Y is a geometrical factor, and G_{craze} is the energy absorbed in forming unit area of new craze. Typically, in well-prepared tensile specimens, σ_{craze} is between 20 and 50 MPa, and crack length a refers to a surface scratch or groove no more than 0.25 μm deep [80]. It follows that G_{craze} must also be small, i.e. between 0.1 and 1 J m^{-2}. This is realistic, because the critical notch-opening displacement δ_{craze} at craze initiation is in the range 10-20 nm, and in a linear elastic material G_{craze} cannot be larger than $\sigma_y\delta_{craze}$.

Like microscopic surface scratches, rubber particles can be effective craze-initiation sites, as numerous experimental studies have shown [1, 71-72]. To act in this way, the rubber particles must first cavitate to form rubber-reinforced spherical holes, in which the rubber provides significant reinforcement only when it is highly strained. In LEFM, spherical voids are treated as penny-shaped or disc cracks [63] lying normal to the tensile direction; they have a geometric factor $Y = 2/\pi$ and crack length $a = D/2$. Equation 15 then becomes:

$$\sigma_{craze} = \sqrt{\frac{\pi\,E\,G_{craze}}{2(1-\nu^2)\,D}} \qquad (16)$$

Figure 7 shows the results of calculations based on equation 16, with E = 2.8 GPa, ν = 0.4, and three different values of G_{craze}. They demonstrate that the critical stress for craze formation is strongly dependent on particle size. It follows that with increasing diameter σ_{craze} must eventually fall below the shear yield stress of the fully-cavitated blend, which is independent of D once the particles have fully cavitated. Because it is controlled by an

energy barrier, void formation in an intact rubber particle is a thermally-activated rate process. Consequently, void formation takes place over a period of time, beginning with primary cavitation in a small fraction of larger particles, which then initiate crazes that propagate radially outwards, producing secondary cavitation and crazing in the particles they encounter. These predictions are supported by optical and transmission electron microscopy studies of multiple crazing in high impact polystyrene (HIPS), ABS and other rubber toughened thermoplastics [1]. Except for HIPS, which shows little sign of ductility under tensile loading, there is ample evidence that crazing in these blends is accompanied by dilatational shear yielding in Izod impact tests, and that increasing particle size tends to promote crazing at the expense of shear yielding. For this reason, manufacturers of ABS, RTPVC, and RTPMMA blends prefer to keep particle sizes well below 1 μm [56].

As noted earlier, multiple crazing does not necessarily lead to immediate fracture. Some well-made HIPS specimens reach extensions as high as 60% by transferring stress to the fibrillated rubber particles. However, this stabilizing mechanism does not operate in all 'super-tough' blends. In many cases, the grafted rubber particles used to toughen polyamides do not contain the rigid inclusions that are necessary for stable fibrillation of the rubber phase in large rubber particles. The benefits of these inclusions are demonstrated in a recent paper, which describes a novel method for producing supertough PA6 blends using quite small amounts of polybutadiene to form thin elastomeric shells around a grafted LDPE core [81]. At a concentration of 20% by weight, these grafted core-shell particles enable the blend to reach an impact energy of 800 J m^{-1}, although particle sizes are approximately 1 μm, and particles of this size introduced by conventional melt compounding almost invariably cause premature fracture. This work demonstrates that ductile-brittle transitions are not determined simply by particle size. The way in which the deformation zone evolves after the rubber particles have cavitated and initial yielding has taken place is also important.

To have a significant effect on fracture behavior, newly-formed crazes must first degrade to form true cracks. This can happen at any stage of loading, but the severity of the problem is reduced by partial load transfer to the rubber particles. The best way to determine whether large rubber particles initiate craze-induced fracture before or after the material has yielded is to study tensile test data for blends with different particle sizes. Ideally, all blends included in the study would have monodisperse particle size distributions, but that condition is extremely

difficult to achieve in extruder-compounded materials like super-tough nylons. In practice, extruder blends with quite small average particle sizes often contain a small percentage of much larger particles, which would be sufficient to induce premature fracture.

Figures 8-10 compare tensile data on two series of nylon/rubber blends, based respectively on a-PA and PA6. Both nylons were compounded with 20% by weight of an ethylene/1-octene copolymer rubber (EOR), which was grafted to the polyamide using maleic anhydride (MA) [2, 52]. Particle sizes were adjusted by using pairs of rubbers with different levels of MA grafting, and by varying processing conditions. In this way it was possible to produce both monodisperse and bimodal size distributions. These studies showed that correlations between Izod impact behavior and particle size were improved by treating each bimodal blend as having a 'split personality', so that it behaves like two separate materials with widely differing D_w. It is therefore appropriate to use two data points to specify the properties of these blends. The same principle has been applied to the elongation data in Figure 10.

Each point in Figures 8-10 represents the average of at least 5 tests on injection-molded bars. Almost all of the 69 materials in the original program reached the yield point. The one exception was an a-PA blend with D_w = 2.4 μm (the largest in the series) which had the very low Izod impact strength of 70 J m^{-2}. Figure 8 shows that σ_y is almost independent of particle size; statistical analysis reveals a modest rise of 1.6 MPa per decade with increasing D_w. Yield stresses are only marginally higher for the a-PA series than for PA6 blends, despite the large difference between the neat matrix materials. A possible explanation is that cavitation took place at a tensile stress of about 50 MPa in both sets of blends, since the particles have similar properties, and that the observed yield stresses of the blends are determined by their cavitation stresses rather than the yield stress of the neat matrix. The experimental scatter in Figure 8 is typical of blends made by melt-compounding, over which it is difficult to exercise stringent quality control.

The data are much more scattered in Figure 9, although each point represents the average of 5 measurements. Elongations at break range from 50% to 200% in sets of blends that have almost the same average particle size. Plotting elongation against the fourth moment of the size distribution does little to reduce the scatter, and the best interpretation that can be placed on these results is that the lower elongations are due to large crack-initiating flaws of various

sizes dispersed randomly in some batches of moldings. The most obvious source of these flaws is the compounding process. According to the crazing model, homogeneous rubber particles larger than about 3 μm would be expected to initiate brittle fracture under the stresses required for cold drawing in PA6 blends, and it is difficult to ensure that no particles of this size are formed during a particular mixing operation. In that respect, tensile specimens pose a harder challenge than Izod bars, because the probability of finding a critical random flaw is much greater along the 50 mm gage length of a tensile bar than in the small notch tip region of an Izod specimen. This principle is embodied in Weibull statistics [82]. Once the average particle size exceeds ~1 μm, particles with 3 μm diameters constitute a substantial component of the regular size distribution, and premature fracture cannot be avoided. Significantly, the blends with the largest average particle sizes have the lowest elongations.

The results presented in Figure 10 display a more coherent pattern of behavior, perhaps because the rheological properties of a-PA melts offer better control over particle size distribution. This pattern is very similar to the one shown in Figure 1: toughness reaches a maximum at D_w = 0.2-0.3 μm, with DB transitions on both sides of the peak. The new model for particle size effects provides an explanation for this behavior. When D_w<0.1 μm, rates of primary rubber particle cavitation are relatively low under a tensile stress of ~50 MPa (σ_m = 16.7 MPa) , and yielding is restricted to localized dilatation bands rather than extending along the whole gage length. On the other hand, when D_w>1 μm the larger particles cavitate and initiate crazes, which then turn into propagating micro-cracks. Maximum toughness is achieved when the particles are large enough to support a reasonably high rate of strain at a moderate yield stress, but not so large that they produce unstable crazes.

Crazing was first observed in rubber-toughened nylons by Flexman [4], who reported ‘craze cracks’ in RTPA66 blends. More recently, crazes have been observed in rubber-toughened PA6 and a-PA blends [52]. They were initiated under impact, in 6.35 mm thick, sharply-notched, three-point bend specimens, using a hammer-stop to limit crack growth. Multiple crazing preceded the highly cavitated shear yield zone by least 1 mm. These observations confirm that the conditions for craze initiation are satisfied under plane strain conditions at stresses below the (constrained) shear yield stress of the 80/20 nylon/EOR blends. The formation of crazes and craze-like deformation bands in rubber-toughened semi-crystalline polymers is discussed in a recent review by Cotterell et al [83].

3. Discussion

The principles outlined above provide a quantitative basis for analyzing the effects of particle size on the fracture behavior of rubber toughened thermoplastics in tests on notched specimens, and hence explaining the ductile brittle transitions illustrated in Figure 1. When rubber particles are very small, they require very large dilatational stresses and strains in order to form internal voids. Consequently, notched specimens are unable to develop a substantial yield zone before crack growth from the notch tip brings the test to an end. By contrast, increasing the particle size causes a reduction in the critical volume strain for cavitation, thereby enabling the plastic zone to expand outward from the notch tip before fracture intervenes. In relatively ductile polymers (polyamides, polypropylene, PVC, etc) this can eventually result in super-tough behavior, provided that the materials properties and test conditions are favorable. Numerous experimental studies demonstrate that problems can arise. Most notably, raising the shear modulus of the rubber phase, by crosslinking, changing chemical composition, or simply reducing the test temperature, increases $\varepsilon_v(cav)$ and reduces fracture resistance [26]. The energy balance model provides a sound theoretical basis for interpreting these effects. In combination with Gurson's equations for yielding in porous solids, it explains why rubber-toughened polymer blends exhibit a lower DB transition.

Hitherto, progress in understanding the upper DB transition has been much slower, basically because the underlying factors responsible for brittle fracture in this region were unclear. The key to understanding this transition is the recently-developed LEFM model for craze initiation, which provides a new perspective on the whole problem. Supertough behavior in polymer blends depends on the development of a substantial porous zone around the notch tip, which does not contain unstable crazes. One way to achieve this optimum result is to avoid craze formation altogether, by keeping particle sizes small, while ensuring that they are not so small that they are excessively resistant to cavitation. On the other hand, crazes are only precursors to true cracks, and an alternative possibility is to design blends in which easily-cavitated rubber particles of moderate size are able to stabilize existing crazes and therefore confer a certain level of toughness on the blend [81]. Very large particles are almost always undesirable.

Figures 11 and 12 show how competition between the various deformation mechanisms affects yield stress and plastic zone size in a model RTPA6 blend. The solid line in Figure 11 denotes σ_{1y}, the critical value of σ_1 at the onset of shear yield, whether before or after cavitation. Under plane strain loading, the stresses (σ_1, σ_2, σ_3) take the form (σ, σ, $2\nu\sigma$) on the crack plane. This enables the critical stresses for cavitation, shear yielding and craze initiation to be compared directly by means of a two-dimensional plot of σ_{1crit} against *log(D)*, although cavitation is controlled by the mean stress, shear yielding is governed by the pressure-modified effective stress, and craze initiation is determined by the applied tensile stress. The cavitation stress curve in this figure is derived from the fitted line in Figure 2, and the craze initiation curve is similar to those shown in Figure 7, with G_{craze} = 0.2 J m^{-2}. Because of the complexity of the interactions between competing micro-mechanisms, no attempt has been made to estimate the yield stress for a combination of crazing and shear yielding.

The highest calculated value of σ_{1y} is 108 MPa. Figure 4 shows that shear yielding takes place in the void-free RTPA6 model blend when the stress on the crack plane reaches (108, 108, 87) MPa. Since cavitation stresses are higher than this when the particles are very small, full constraint is maintained all the way to the point at which a crack initiates from the notch tip. Therefore in blends with D>0.03 μm brittle fracture occurs with minimum energy dissipation, K_{IC} is low (~ 1 MPa m$^{0.5}$) and r_p is <0.03 mm. By contrast, increasing the particle size above 0.03 μm enables the blend to cavitate before fracture intervenes, thereby causing a reduction in σ_{1y}, the principal stress at yield on the crack plane, which eventually falls to 55.8 MPa at D = 0.078 μm. At larger values of D, the cavitation stress falls below the shear yield stress of the fully-cavitated blend, and the plane-strain shear yield stress is no longer a function of particle size. This is the super-tough region, with K_I exceeding 3.5 MPa m$^{0.5}$, and plastic zone sizes of at least 1.0 mm. Dilatational shear yielding remains the dominating deformation mechanism until the onset of the ductile-brittle transition at $D = D_{DBo}$ = 0.35 μm, which occurs when the craze initiation curve crosses the shear-yield line.

Beyond this point, craze-induced brittle fracture becomes a possibility, and the extent of crack tip yielding prior to fracture is minimized. The location of this transition can be calculated by rearranging equation 16, as follows:

$$D_{DBo} = \frac{\pi E G_{craze}}{2(1-\nu^2)\sigma_{ycav}^2} \qquad (17)$$

where σ_{ycav} is the yield stress of the fully cavitated blend (56 MPa in Figure 11). This equation explains in general terms why Wu observed a shift in the critical particle size when he increased the rubber content of his PA66 blends from 10% to 25%. Adding rubber causes both Young's modulus and yield stress to fall, but the yield behavior of the blend is dominated by the decrease in σ_{ycav}, which shifts D_{DBo} upwards.

Figure 12 shows the relationship between D and r_p, calculated using equation 3 with data on σ_{1y} taken from Figure 11. Irwin's correction has been applied in all cases to allow for stress redistribution [66]. As the data do not extend beyond D = 0.35 μm, the reduction in toughness observed at larger particle sizes is represented by dotted lines which are at best approximations to the plastic zone sizes seen in fracture mechanics specimens.

It should be noted that the calculations used in preparing the Figures 11 and 12 are based on hypothetical blends with very narrow distributions of particle size, deforming under isothermal conditions. Polydispersity introduces additional complications, which have been discussed briefly in previous sections, and adiabatic energy dissipation is an important issue in notched impact tests on supertough blends. For purposes of illustration, the calculations are based on a particular 80/20 PA6/rubber blend with specific properties, measured at room temperature under low rates of strain. However, charts similar to Figures 11 and 12 could be generated to represent other test conditions and materials properties; the permutations are endless.

Another limitation of the illustrations is that they define the boundaries between linear elastic behavior and inelastic responses at an early stage in the fracture test. This simplified approach identifies conditions for the onset of the three main deformation micro-mechanisms, but is unable to determine in any detail how the deformation zone subsequently develops. The insights obtained in this way are valuable, but much remains to be done; the principles set out in this introductory paper open up the subject to further exploration. Later papers in this series will address other aspects of particle size dependence in rubber-toughened thermoplastics. The most obvious issues are the effects of rubber content, test temperature, strain rate, and materials properties. Looking a little further afield, a similar LEFM-based

approach to DB transitions can be applied to blends containing mineral filler particles, which form voids by debonding, and to rubber toughened thermosetting resins, in which large cavitated particles form microcracks rather than crazes.

As noted earlier, another topic to be addressed is the response of notched Izod specimens during the later stages of the test, well beyond the onset of dilatational yielding or crazing. Initial events are extremely important in determining the subsequent behavior of the specimen, but in very tough blends most of the energy is absorbed during notch tip blunting and crack propagation, where non-isothermal deformation is known to affect energy absorption [84-90].

On a more fundamental level, this paper raises basic questions about the susceptibility of different thermoplastics to craze initiation, which can now be seen to depend on the value of G_{craze}. Studies by Vincent [91] and more recently by Wool [92] show that the strength of a thermoplastic is ultimately dependent on the cross-sectional area of its chains. Thus the LEFM model for craze initiation establishes a link between chemical structure and DB transitions in polymer blends, which deserves further exploration.

4. Conclusions

This paper introduces a new model for deformation, yield and fracture of polymer blends in the plane strain region close to a notch tip, which overcomes the deficiencies of the inter-particle approach advocated by Wu [5-6]. It employs linear elastic fracture mechanics in combination with earlier models for rubber particle cavitation, shear yielding and craze initiation to determine the order in which these mechanisms are activated when a notched specimen is loaded, and to map their spread from the notch tip. Calculations for a specific 80/20 nylon/rubber blend show that when the rubber particles have very small diameters (D <0.03 μm) they are unable to cavitate because the critical stress for cavitation lies above the (constrained) shear yield stress of the blend, which is itself extremely high. It is possible that a minute shear yield zone is formed, but the stresses in this zone are so high that the essential failure mechanism is craze initiation and brittle fracture from the notch tip. By contrast, increasing D above about 0.03 μm enables the particles to cavitate before the material yields, and consequently reduces the shear yield stress, which at this stage is a function of the volume fraction of cavitated particles. Over a size range running approximately from 0.03 μm

to 0.08 μm, the shear yield stress is controlled by the cavitation stress, and increasing *D* produces a continuous decrease in σ_{1y}, which leads to a rapid increase in toughness. Eventually, the cavitation stress falls below the shear yield stress of the fully-cavitated blend, and toughness reaches a maximum.

A less desirable result of increasing particle size is that it reduces the critical stress for craze initiation, because large cavitated particles act as very effective Griffith flaws. Formation and subsequent failure of crazes causes fracture of the yield zone before it has fully developed. If the particles are very large (e.g. D>10 μm) and $\sigma_{craze} << \sigma_{1y}$, the extent of shear yielding will be minimal, and brittle fracture will ensue. If on the other hand σ_{craze} is quite close to σ_{1y}, a more likely outcome is extensive shear yielding with some associated crazing, followed by premature fracture at reduced elongation. Under these conditions, the critical notch-tip opening displacement is only slightly lower than the optimum, and there is only a modest reduction in energy to break.

For purposes of illustration, calculations presented in this paper relate to a series of blends with very narrow distributions of particle size, which have tensile yield stresses of about 50 MPa, and other mechanical properties as listed in the text. The properties chosen correspond roughly with those of PA6/rubber blends with a volume ratio of 74/26 (weight ratio 80/20), measured at room temperature and at a low strain rate. The ductile-brittle transitions represented in Figures 11 and 12 were obtained by inserting these specific data into the relevant equations of the model, and their locations will obviously shift if different data are used. It follows that DB transitions would be expected to vary with rubber content, as observed by Wu [5-6], with temperature, as reported by Borggreve et al [8], and with strain rate. Later papers in this series will explore these and other factors affecting DB transitions in polymer blends.

Acknowledgment

The authors dedicate this paper to the memory of their friend and colleague, Dr. Henno Keskkula, who had a long-lasting interest in the issues addressed in this study.

References

1. Bucknall CB. Toughened Plastics. London: Applied Science Publishers, 1977.
2. Huang JJ, Keskkula H, Paul DR. Polymer 2006;47(2):639-651.
3. Epstein B. US Patent No 4,174,358: E I DuPont, 1979.
4. Flexman EA. Polym Eng Sci 1979;19:564-571.
5. Wu S. J Polym Sci, Polym Phys Ed 1983;21:699-716.
6. Wu S. Polymer 1985;26(12):1855-1863.
7. Hobbs SY, Bopp RC, Watkins VH. Polym Eng Sci 1983;23(7):380-389.
8. Borggreve RJM, Gaymans RJ, Schuijer J, Ingen-Housz JF. Polymer 1987;28(9):1489-1496.
9. Borggreve RJM, Gaymans RJ, Luttmer AR. Makromol Chem, Macromol Symp 1988;16:195-207.
10. Borggreve RJM, Gaymans RJ. Polymer 1989;30(1):63-70.
11. Borggreve RJM, Gaymans RJ, Schuijer J. Polymer 1989;30(1):71-77.
12. Borggreve RJM, Gaymans RJ, Eichenwald HM. Polymer 1989;30(1):78-83.
13. Gaymans RJ, Borggreve RJM, Oostenbrink AJ. Makromol Chem, Macromol Symp 1990;38:125-136.
14. Oshinski AJ, Keskkula H, Paul DR. Polymer 1992;33(2):268-283.
15. Oshinski AJ, Keskkula H, Paul DR. Polymer 1992;33(2):284-293.
16. Takeda Y, Paul DR. J Polym Sci, Part B: Polym Phys 1992;30(11):1273-1284.
17. Majumdar B, Keskkula H, Paul DR. Polymer 1994;35(7):1386-1398.
18. Majumdar B, Keskkula H, Paul DR. Polymer 1994;35(7):1399-1408.
19. Majumdar B, Keskkula H, Paul DR. Polymer 1994;35(25):5453-5467.
20. Majumdar B, Keskkula H, Paul DR. Polymer 1994;35(25):5468-5477.
21. Majumdar B, Keskkula H, Paul DR, Harvey NG. Polymer 1994;35(20):4263-4279.
22. Oshinski AJ, Keskkula H, Paul DR. Polymer 1996;37(22):4891-4907.
23. Oshinski AJ, Keskkula H, Paul DR. Polymer 1996;37(22):4909-4918.
24. Oshinski AJ, Keskkula H, Paul DR. Polymer 1996;37(22):4919-4928.
25. Oshinski AJ, Keskkula H, Paul DR. J Appl Polym Sci 1996;61(4):623-640.
26. Gaymans RJ. In: Paul DR, Bucknall CB, editors. Polymer Blends 2nd edition, vol. 2. New York: Wiley, 2000.
27. Hage E, Hale W, Keskkula H, Paul DR. Polymer 1997;38(13):3237-3250.
28. Hale W, Keskkula H, Paul DR. Polymer 1999;40(2):365-377.
29. Hale W, Keskkula H, Paul DR. Polymer 1999;40(12):3353-3365.
30. Hale W, Lee JH, Keskkula H, Paul DR. Polymer 1999;40(13):3621-3629.
31. Jang BZ, Uhlmann DR, Vander Sande JB. J Appl Polym Sci 1984;29(11):3409-3420.
32. Jang BZ, Uhlmann DR, Vander Sande JB. Polym Eng Sci 1985;25(10):643-651.
33. Jiang W, Tjong SC, Li RKY. Polymer 2000;41(9):3479-3482.
34. Liang JZ, Li RKY. J Appl Polym Sci 2000;77(2):409-417.
35. Jiang W, Yu DH, An LJ, Jiang BZ. J Polym Sci, Part B: Polym Phys 2004;42(8):1433-1440.
36. Margolina A, Wu S. Polymer 1988;29(12):2170-2173.

37. Sjoerdsma SD. Polym Comm 1989;30(4):106-108.
38. Liu ZH, Li RKY, Tjong SC, Qi ZN, Wang FS, Choy CL. Polymer 1998;39(18):4433-4436.
39. Liu ZH, Zhang XD, Zhu XG, Qi ZN, Wang FS, Li RKY, Choy CL. Polymer 1998;39(21):5047-5052.
40. Liu ZH, Li RKY, Tjong SC, Choy CL, Zhu XG, Qi ZN, Wang FS. Polymer 1999;40(11):2903-2915.
41. Jiang W, Yu DH, Jiang BZ. Polymer 2004;45(19):6427-6430.
42. Jiang W, Hu YX, Yin JH. J Polym Sci, Part B: Polym Phys 2008;46(7):766-769.
43. Dijkstra K, Tenbolscher GH. J Mater Sci 1994;29(16):4286-4293.
44. Huang JJ, Keskkula H, Paul DR. Polymer 2006;47(2):624-638.
45. Dompas D, Groeninckx G. Polymer 1994;35(22):4743-4749.
46. Dompas D, Groeninckx G, Isogawa M, Hasegawa T, Kadokura M. Polymer 1994;35(22):4750-4759.
47. Dompas D, Groeninckx G, Isogawa M, Hasegawa T, Kadokura M. Polymer 1994;35(22):4760-4765.
48. Muratoglu OK, Argon AS, Cohen RE, Weinberg M. Polymer 1995;36(5):921-930.
49. Muratoglu OK, Argon AS, Cohen RE, Weinberg M. Polymer 1995;36(25):4771-4786.
50. Muratoglu OK, Argon AS, Cohen RE. Polymer 1995;36(11):2143-2152.
51. Argon AS, Bartczak Z, Cohen RE, Muratoglu OK. In: Pearson RA, Sue HJ, Yee AF, editors. Toughening of Plastics, ACS Symposium Series, vol. 759. Washington DC: American Chemical Society, 2000.
52. Huang JJ, Paul DR. Polymer 2006;47(10):3505-3519.
53. Corte L, Beaume F, Leibler L. Polymer 2005;46(8):2748-2757.
54. Corte L, Leibler L. Macromolecules 2007;40(15):5606-5611.
55. Lutz JT, Dunkelberger DL. Impact Modifiers for PVC: The History and Practice. New York: Wiley, 1992.
56. Cruz-Ramos CA. Polymer Blends. In: Paul DR, Bucknall CB, editors., vol. 2. New York: Wiley, 2000.
57. Cheng CM, Hiltner A, Baer E, Soskey PR, Mylonakis SG. J Appl Polym Sci 1994;52(2):177-193.
58. Lombardo BS, Keskkula H, Paul DR. J Appl Polym Sci 1994;54(11):1697-1720.
59. Wildes G, Keskkula H, Paul DR. Polymer 1999;40(25):7089-7107.
60. Robeson LM. Polymer Blends: A Comprehensive Review. Munich: Hanser, 2007.
61. Westergaard H. J Appl Mech 1939;61A:49-53.
62. Broek D. Elementary Engineering Fracture Mechanics. Dordrecht, Netherlands: Martinus Nijhoff, 1986.
63. Williams JG. Fracture Mechanics of Polymers. Chichester UK: Ellis Horwood, 1987.
64. Anderson TL. Fracture Mechanics: Fundamentals and Applications, 3rd edn. Boca Raton FL: CRC Press, 2005.
65. Gdoutos EE. Fracture Mechanics: An Introduction. Dordrecht, Netherlands: Springer Verlag, 2005.
66. Irwin GR. Sagamore Research Conference Proceedings 1961;4:63-78.
67. Thomason PF. Ductile Fracture of Metals. New York: Pergamon Press, 1990.
68. Lazzeri A, Bucknall CB. J Mater Sci 1993;28(24):6799-6808.
69. Bucknall CB, Karpodinis A, Zhang XC. J Mater Sci 1994;29(13):3377-3383.
70. Lazzeri A, Bucknall CB. Polymer 1995;36(15):2895-2902.

71. Bucknall CB. Chapter 22. In: Paul DR, Bucknall CB, editors. Polymer Blends, vol. 2. New York: Wiley, 2000.
72. Bucknall CB. In: Haward R N, Young RJ, editors. The Physics of Glassy Polymers, 2nd edition. London: Chapman & Hall, 1997.
73. Bucknall CB, Ayre DS, Dijkstra DJ. Polymer 2000;41(15):5937-5947.
74. Ward IM. Mechanical Properties of Solid Polymers, 2nd edition. New York: Wiley, 1983.
75. Gurson AL. In: Taplin DMR, editor. ICF4 Fracture 1977, vol. 2A. Oxford: Pergamon, 1977.
76. Gurson AL. J Eng Mater Technol, Trans ASME 1977;99(1):2-15.
77. Guild FJ. In: Paul DR, Bucknall CB, editors. Polymer Blends, vol. 2. New York: Wiley, 2000.
78. Sue HJ. J Mater Sci 1992;27(11):3098-3107.
79. Bucknall CB. Polymer 2007;48(4):1030-1041.
80. Argon AS, Hannoosh JG. Philos Mag 1977;36(5):1195-1216.
81. Ke Z, Shi D, Yin J, Li RKY, Mai YW. Macromolecules 2008;41(20):7264-7267.
82. Weibull W. J Appl Mech 1951;18:293-305.
83. Cotterell B, Chia JYH, Hbaieb K. Eng Fracture Mech 2007;74(7):1054-1078.
84. Dijkstra KD, Gaymans RJ. J Mater Sci 1994;29(12):3231-3238.
85. van der Wal A, Gaymans RJ. Polymer 1999;40(22):6067-6075.
86. Inberg JPF, Takens A, Gaymans RJ. Polymer 2002;43(9):2795-2802.
87. Zuiderduin WCJ, Vlasveld DPN, Huetink J, Gaymans RJ. Polymer 2004;45(11):3765-3779.
88. Dijkstra PTS, Gaymans RJ, Van Dijk DJ, Huetink J. Polym Eng Sci 2003;43(9):1613-1623.
89. Zuiderduin WCJ, Westzaan C, Huetink J, Gaymans RJ. Polymer 2003;44(1):261-275.
90. Zuiderduin WCJ, Huetink J, Gaymans RJ. Polymer 2006;47(16):5880-5887.
91. Vincent PI. Polymer 1972;13(12):558-560.
92. Wool RP. J Polym Sci, Part B: Polym Phys 2005;43(2):168-183.

Figure Captions

Figure 1. Relationship between particle size and impact behaviour for a typical 'super-tough' thermoplastic blend. Points **b** and **d** mark lower (•) and upper (o) ductile-brittle transitions. Schematic representation based broadly on data of Huang et al for a series of 80/20 RTPA6 blends [2].

Figure 2. Effect of rubber particle size on critical volume strain and critical mean stress at cavitation. Data obtained by Dompas et al in tests on transparent PVC/MBS blends [46]. Dotted line calculated using energy balance model, equation 6, with ε_v constant. Solid line is parallel to dotted line, but shifted upwards by a factor of 2.1 to fit data.

Figure 3. Map of cavitated zone in plane strain region, showing dependence of zone boundary on particle diameter when K_I = 1 MPa $m^{0.5}$. Critical mean stresses calculated using equations 2a-2d with bulk modulus K_b = 3 GPa and data from solid curve in Figure 2.

Figure 4. Comparison between pressure modified von Mises criterion for a void-free blend (equation 7 with μ = 0.36) and pressure-modified Gurson criterion for the same blend, now fully-cavitated (equation 11).

Figure 5. Effect of low modulus inclusions (voids or solid rubber particles) on tensile yielding in dry PA6, and of voids on band angle (alternating dashes and dots)[68]. Data points from Huang et al [2].

Figure 6. Pressure-dependent von Mises yield envelopes under plane stress and plane strain loading, with K_I = 1.0 MPa $m^{0.5}$, for void-free 80/20 PA6/rubber blend with Poisson's ratio ν = 0.4, pressure coefficient μ = 0.36.

Figure 7. Critical tensile stress for craze initiation as a function of (cavitated) rubber particle diameter, calculated using equation 16 with three different values of G_{craze}, the specific energy of craze initiation.

Figure 8. Yield stresses of dry 80/20 a-PA and PA6 blends over a range of particle sizes at 23°C. Horizontal lines indicate yield stresses of neat a-PA and PA6 in dry state. Data of Huang et al [2].

Figure 9. Tensile elongation at break of dry PA6 blends containing 20% by weight of ethylene-octene rubber. Data of Huang et al [2].

Figure 10. Tensile elongation at break of dry a-PA blends containing 20% by weight of ethylene-octene rubber. Data of Huang et al [2]. Open circles denote blends with monodisperse particle size distribution. Closed squares denote bimodal distributions, with each blend represented twice, to show upper and lower peaks in the size distribution separately.

Figure 11. Schematic diagram illustrating effects of particle size on deformation mechanisms close to the crack plane ($\theta = 0$) under plane strain conditions, in 80/20 RTPA6 blend. Craze line calculated using equation 16 with E = 2.8 GPa and G_{craze} = 0.2 J/m^2. Shear yield stresses calculated using equation 7, with pressure coefficient μ = 0.36 (see Figure 4). Solid line defines critical stress for shear yielding, both with and without prior cavitation. Note that crazing and shear yielding can take place simultaneously in tough specimens containing relatively large particles.

Figure 12. Plane strain plastic zone radius at $\theta = 0$, calculated using equation 3 with r_p doubled (Irwin's correction factor [64, 66]). Yield stress data taken from Figure 11, on the assumption that the shear yield zone is fully developed. At large particle sizes, craze formation increases the probability that the specimen fails through crack initiation in regions of high local stress. Dotted lines are estimates based very roughly on observed reductions in fracture resistance of notched specimens.

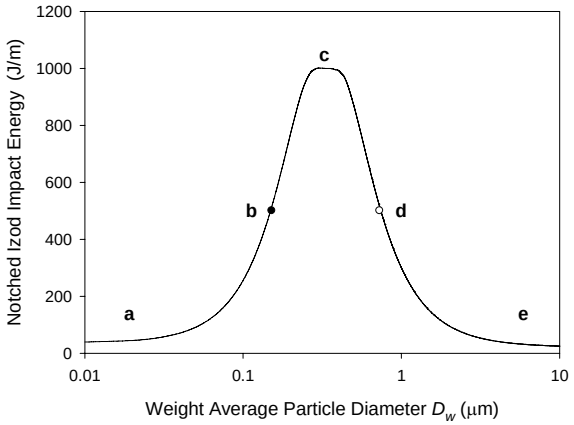

Figure 1

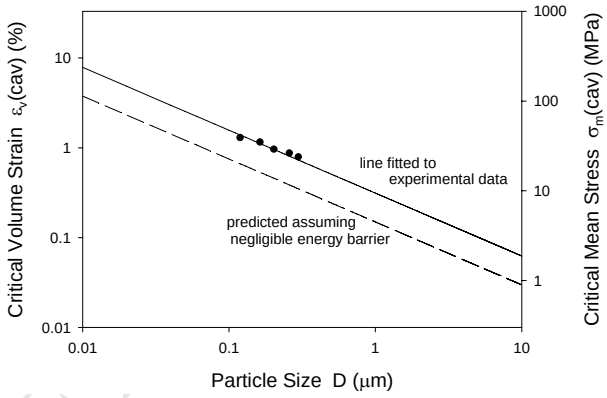

Figure 2

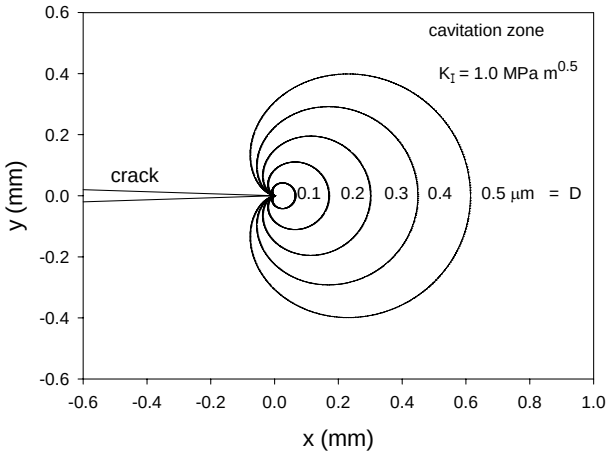

Figure 3

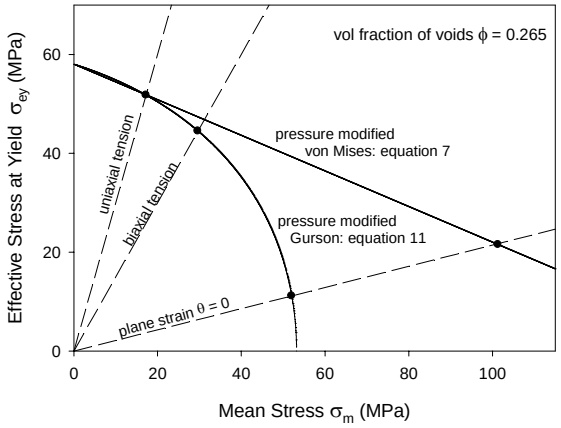

Figure 4

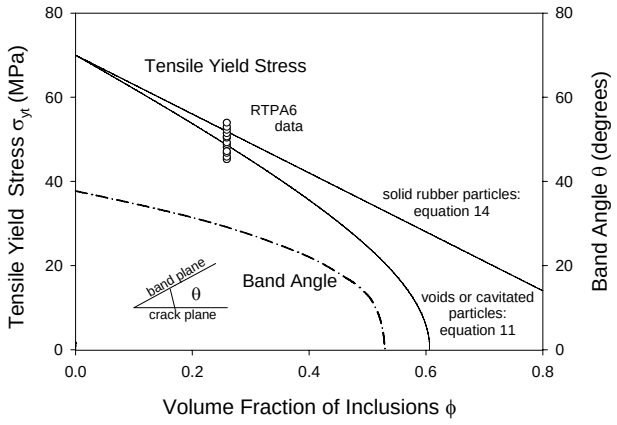

Figure 5

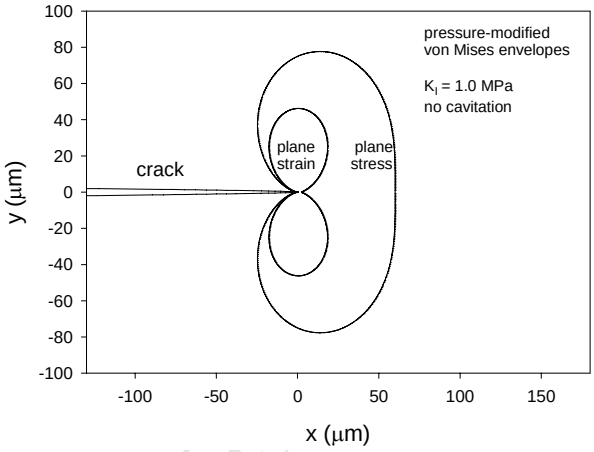

Figure 6

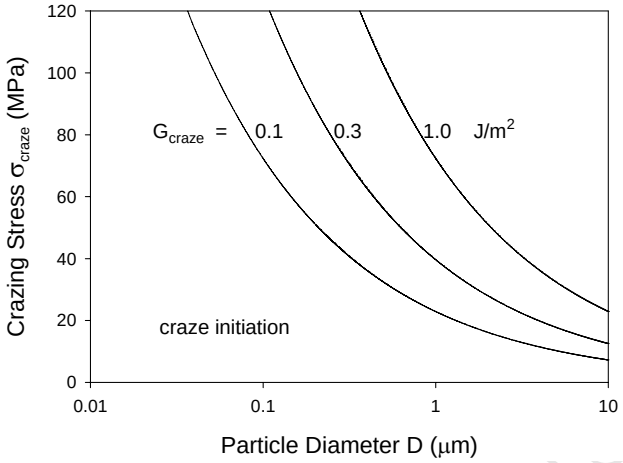

Figure 7

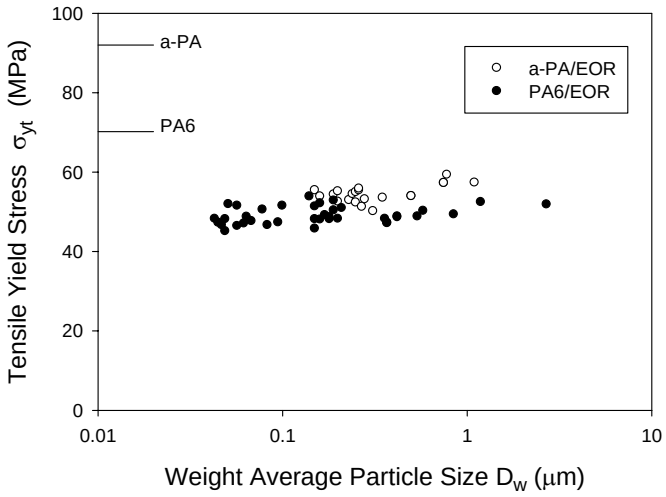

Figure 8

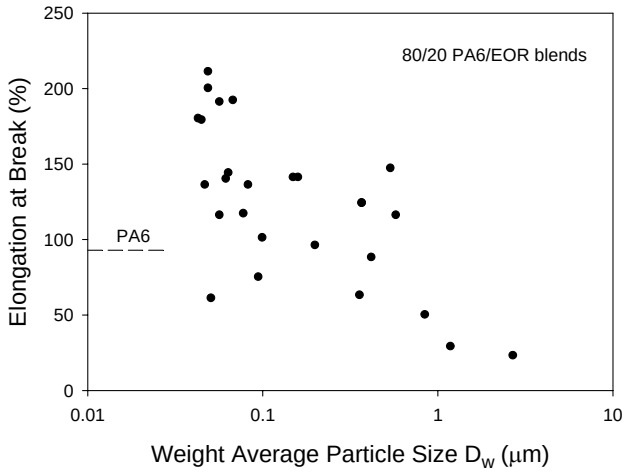

Figure 9

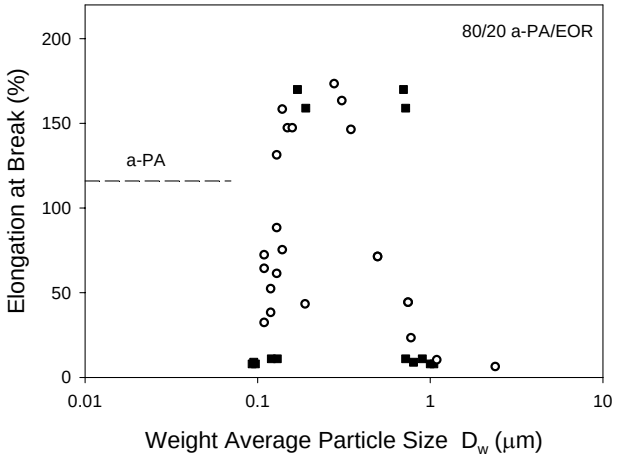

Figure 10

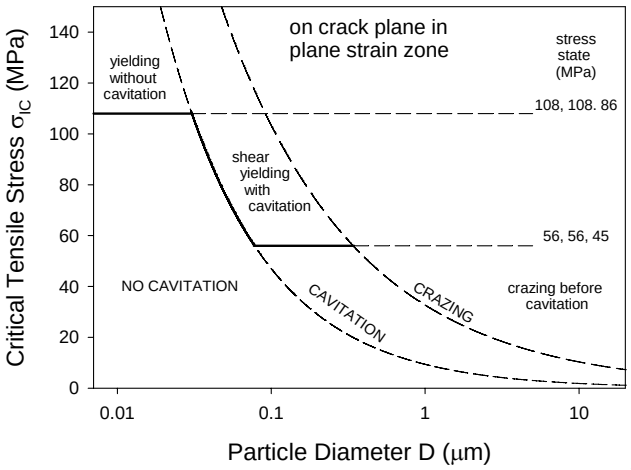

Figure 11

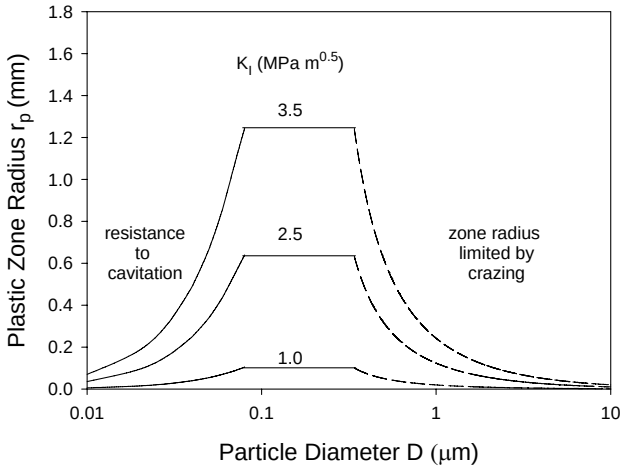

Figure12

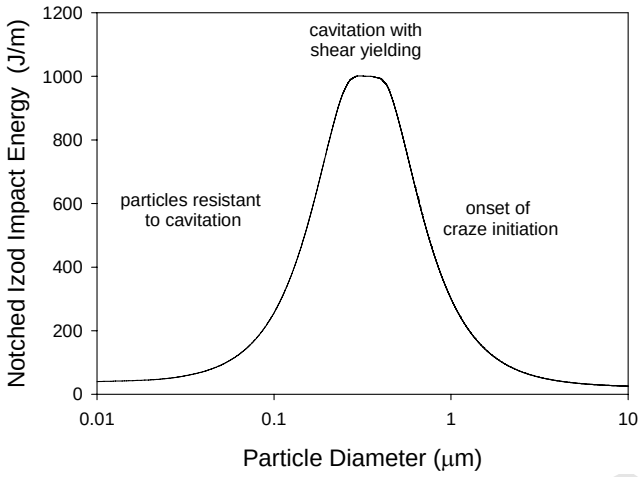

Table of Content Graphic